Imaging ring-current wave packets in the helium atom

J. Venzke, A. Becker, and A. Jaron-Becker
JILA and Department of Physics, University of Colorado, Boulder, Colorado 80309-0440, USA

(Received 20 August 2020; accepted 22 March 2021; published 5 April 2021)

We study the reconstruction of a wave packet and the corresponding electron dynamics in an atom via photoelectron angular distributions (PADs) in a pump-probe scheme as a function of time delay. The method is applied to the superposition of ground and one or two excited states in helium atom representing field-free charge migrations on the attosecond timescale in form of ring currents around the core. It is based on the interference between one- and two-photon transitions from ground and excited states into the continuum. In the reconstruction predictions of first- and second-order perturbation theory are used to determine the unknown phases and amplitudes from the PADs, which we simulate via solutions of the time-dependent Schrödinger equation in single-active-electron approximation. Results of calculations show that the reconstruction technique works well for peak laser intensities less than 10^{13} W/cm^2. Knowledge of the electric field of the probe pulse is required with shot-to-shot variations of carrier-to-envelope phase and peak intensity of up to 10% and 20%, respectively. The relevance of different one- and two-photon pathways for the reconstruction as a function of peak intensity and pulse duration is analyzed—specifically their role for ultrashort probe pulses with broad bandwidths.

DOI: 10.1103/PhysRevA.103.042808

I. INTRODUCTION

The availability of ultrafast light sources at wavelengths from the vacuum ultraviolet (VUV) and extreme ultraviolet (EUV) to the soft-x-ray regime via the technologies of free electron lasers (FELs) [1] and high-order harmonic generation (HHG) [2,3] has opened a new regime of ultrafast measurements in atomic and molecular physics. Laser pulses of duration as short as a few tens of attoseconds have been demonstrated experimentally [4,5] and enabled the observation of electron dynamics (for recent reviews, see Refs. [6–11]). One example is the time-resolved measurement of the photoelectric effect in atoms and solids [12–16]. Electron emission from the target has been also temporally resolved for a transition of the electron into the continuum through excited-state resonances [17–19], autoionizing states [20–22], Fano resonances [23–26], and for correlated electron emission [27–29]. Electron wave-packet dynamics in superposition states of atoms and molecules has been another focus of ultrafast time-resolved studies, either for single valence electron motion [30–41] or correlated two-electron dynamics [42–44].

Recently, the application range of ultrafast laser pulse technology has been extended by the capability to control the polarization of the emitted light in high-order harmonic generation and free-electron lasers. The physical principle to produce circularly polarized high-order harmonics has been proposed and applied first two decades ago [45]. Efficient phase matching of the generated light in the EUV and soft x-ray regime [46–48] and the control of the polarization stage [49] has been demonstrated more recently. Similarly, free-electron laser light with variable polarization has become available [50,51]. The potential to control the polarization and helicity of light generated by HHG and FELs extends the range of accessible states and transition pathways during photon absorption. States with varying orbital angular momentum and magnetic quantum number can be excited during the interaction with the pulses. In turn, the helicity of the light pulses can be used to selectively prepare superpositions of states in atoms or molecules with a variety of combinations in the quantum numbers (principal, orbital angular momentum, magnetic) on an ultrafast timescale.

One of the simplest cases of a superposition of atomic states with different orbital angular momentum and magnetic quantum numbers is that of a helium atom in the $1s$ and $2p_1$ states. It results in an ultrafast electron dynamics given by a wave packet rotating in a plane around the nucleus with a period of ≈200 attoseconds. We use this dynamics as a prototype example to study the reconstruction of the corresponding wave packet via ionization with an ultrashort linearly polarized probe laser pulse. To this end, we analyze the photoelectron angular distributions as a function of time delay from the instant of preparation of the atomic superposition states. The concept is based on the idea to utilize quantum beating signals, where the imaged wave packet is interfered with a reference wave to reconstruct a wave function [31,36,40,52–54]. Accounting for the phase accumulation, ionization cross sections, and characterization of the reference wave packet that is used in the measurement is a nontrivial task. In this work we present a method for wave-packet reconstruction based on quantum beating signals that utilizes perturbation theory. Since the method requires knowledge of the average values for intensity, carrier-to-envelope phase, and pulse duration of the probe pulse, we perform a

sensitivity study to show the impacts of noise produced in an experiment and the limits in peak laser intensity on the reconstruction method. Finally, we consider the extension of the method to imaging of wave packets consisting of superpositions of more than two states.

The rest of the paper is organized as follows: In Sec. II we first present and discuss the ionization scheme on which the reconstruction method is based. Then we briefly review the methods for the numerical solution of the time-dependent Schrödinger equation and the perturbation theory formalism used for the reconstruction algorithm. In Sec. III we present the application of the method to the reconstruction of a circular wave packet in a helium atom. Aspects of the error analysis with respect to the accuracy of the observation of the PADs and the variation of the laser parameters will be presented. Furthermore, the impact of different pathways on the reconstruction process will be studied. Finally, we briefly discuss the extension of the method to superpositions of more than two states along with results for a specific three-state superposition. The paper ends with a summary. We use Hartree atomic units $e = m_e = \hbar = 1$ if not mentioned otherwise.

II. CONCEPT AND THEORETICAL METHODS

A. Pump-probe scheme

In this study, we focus on the reconstruction of a wave function and the related imaging of the dynamics via photoelectron angular distributions (PADs). To this end, we start our simulations in a superposition state of the atom. An experiment will require a pump pulse to generate the superposition. There are a few requirements for the pump pulse itself to apply the reconstruction scheme. Since the scheme relies on the measurement of the PADs at various time delays between the pump and the probe pulse, the pump must be a reproducible pulse with a fixed carrier envelope phase (CEP) such that the superposition generated for each measurement is very similar from shot to shot if not the same. However, the form of the electric field of the pump pulse does not need to be known. Next, the delay between the pump and probe pulses must be controlled on the attosecond timescale to allow for measurements as a function of the delay. The shot-to-shot measurements should be taken for time delays within one cycle of the probe pulse giving rise to the requirement of an attosecond control over the delay. The total delay is irrelevant as long as the two pulses do not overlap in time and the state to be imaged does not decay. Furthermore, photoelectrons generated by the pump pulse have to be separated from those produced by the probe pulse. It might be therefore useful to limit ionization by the pump pulse.

The method studied here can be applied to simple superpositions, consisting of population in two or three atomic states. As prototypical example we consider a helium atom in a $1s$-$2p_1$ superposition, which represents a circular wave packet rotating around the nucleus. This superposition with equal population in the two levels can be created with an $\approx$23 cycle laser pulse at 10^{14} W/cm^2 tuned to the resonance frequency. Figure 1(a) shows the dynamics via isosurfaces of the wave function (i.e., $|r\Psi|^2$) rotating in the x-y plane on an attosecond timescale.

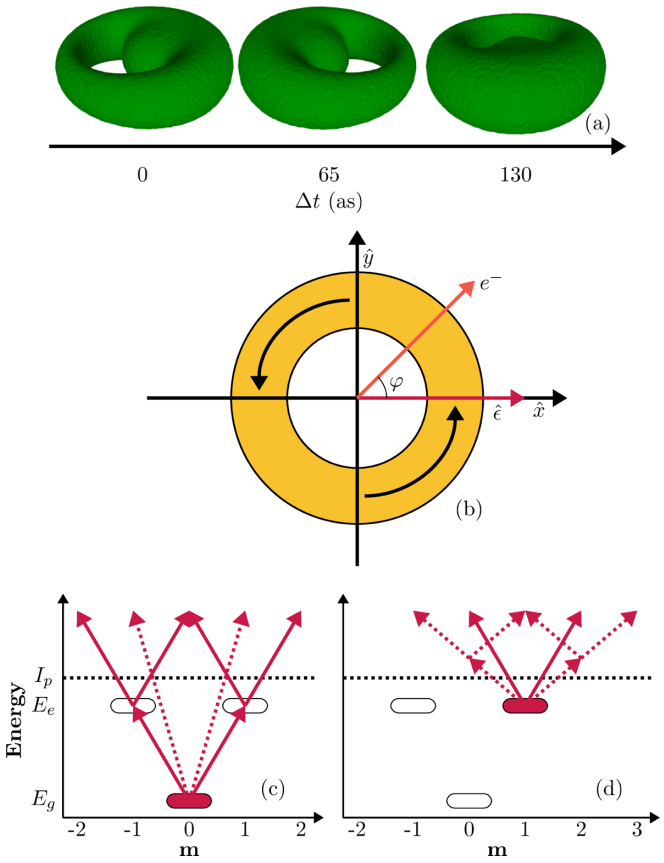

FIG. 1. (a) Isosurfaces of the $1s$-$2p_1$ wave function ($|r\Psi|^2$ is shown) evolving in time. (b) Ionization scheme in the x-y plane. The laser polarization along the x axis is depicted in red, the direction of the ionized electron is shown in orange, and the charge migration is shown in yellow. Selection rules for (c) ground-state signal and (d) excited-state signal. The solid lines illustrate the transitions of photons absorbed at the central frequency and the dashed lines show the pathways for short pulse effect due to the large bandwidth of an ultrashort pulse.

To characterize the motion, and in turn reconstruct the wave function, we expand the initial wave function in the eigenbasis of stationary states and write the wave function at some time t as

$$\Psi(\boldsymbol{r}, t) = a_0\psi_0(\boldsymbol{r}, t) + \sum_{j=1}^{N-1} a_j e^{i\theta_j}\psi_j(\boldsymbol{r}, t), \tag{1}$$

where a_j is a positive real number, θ_j is a relative phase, and $\{\psi_j = \Psi_{nlm};\ j = 0, \ldots, N-1\}$ is the eigenstate basis. While the basis may contain an infinite number of eigenstates, for practical means in the numerical calculations and any application it has to be truncated at some finite number N. Thus, the wave function depends on $N-1$ phases and N amplitudes since the global phase is not a physically relevant quantity. In this framework, all time dependence is contained in the states $|\psi_j(t)\rangle$ and the initial wave function is completely reconstructed if all a_j and θ_j for $j \geqslant 1$ are obtained since a_0 is fixed by the normalization and we set the phase of ground state $|\psi_0\rangle$ to zero. If the wave function generated by the pump pulse

can be reconstructed at a given time, the full time-dependent motion of the wave function has also been obtained.

In the reconstruction scheme that we consider the electron dynamics is probed via ionization by an intense ultrashort laser pulse as a function of time delay after the end of the pump pulse. In the scheme, predictions of first- and second-order perturbation theory (PT) are used to determine the unknown phases and amplitudes from the photoelectron angular distributions (PADs). The latter may be determined in an experiment but in this theoretical study we utilize *ab initio* numerical calculations. For the case of a helium atom in a $1s$-$2p_1$ superposition, we apply a probe laser pulse linearly polarized along the x axis and detect the photoelectron angular distribution in the x-y plane, i.e., for $\theta = \pi/2$, as a function of the angle φ from the x axis, as shown in Fig. 1(b). The absorption of a photon will induce transitions with $\ell \to \ell \pm 1$ and $m \to m \pm 1$ due to the selection rules. The pathways from the ground and the excited state are shown in Figs. 1(c) and 1(d), respectively. The solid arrows represent the pathways for the transitions at the central frequency of the probe pulse. I_p is the ionization potential and the ovals indicate possible resonances. Since we analyze photoelectron emission induced by ultrashort pulses, we need to consider additional pathways due to the broad bandwidth of the pulse [55]. These pathways are the ionization from the ground state with a single photon and the two-photon transition from the excited state, which are represented by the dotted arrows in Fig. 1. Since states in the continuum with the same energy and quantum numbers can be reached via different pathways, the photoelectron angular distribution will change in both shape and yield as the relative amplitudes and phases of each signal varies.

B. Numerical solution of time-dependent Schrödinger equation

To test the applicability and limits of the reconstruction method we use numerical solutions of the time-dependent Schrödinger equation (TDSE) as a substitute for actual measurements of the photoelectron angular distributions. We consider the TDSE in length gauge and single-active electron approximation:

$$i\frac{\partial}{\partial t}\Psi(\mathbf{r},t) = \left[-\frac{\nabla^2}{2} - \mathbf{E}(t)\cdot\mathbf{x} + V(r)\right]\Psi(\mathbf{r},t), \quad (2)$$

where $V(r)$ is a single-active electron potential for helium atom given by [56]

$$V(r) = -\frac{1}{r} - \frac{e^{-2.0329r}}{r} - 0.3953e^{-6.1805r}. \quad (3)$$

giving a ground-state energy of $-0.944\,409$ a.u. and a $2p$ energy of -0.12847 a.u. The potential has been constructed for benchmark tests between TDSE and time-dependent density-functional theory (TDDFT) calculations [56]. The energies match those of the corresponding DFT potential while the experimental values for the ground and the $2p$ state in helium are -0.9037 a.u. and -0.12382 a.u.

For the solution we have expanded $\Psi(\mathbf{r},t)$ in spherical harmonics up to $l_{\max} = |m_{\max}| = 20$ and discretized the radius using fourth-order finite differences. The wave function has been propagated in time with a time step of 0.01 a.u. on a grid with spacing of 0.05 a.u., with a maximum radius of 300 a.u. and an exterior complex scaling on the outer 30 a.u. of the grid utilizing the Crank-Nicolson method for time propagation. The numerical code tested against previously used codes as well as results from numerical calculations published in the literature [57].

To avoid unphysical effects in the numerical simulations we make sure that the electric field integrates to zero by setting the vector potential as [58]

$$A(t) = \begin{cases} A_0 \sin^2\left(\frac{\pi t}{T}\right)\sin\left[w_A\left(t - \frac{T}{2} + \tau_d\right)\right], & 0 \leqslant t \leqslant T \\ 0 & \text{otherwise,} \end{cases} \quad (4)$$

where $A_0 = \frac{c\sqrt{I}}{\omega_A}$, $T = \frac{2\pi N}{\omega_A}$, τ_d is the pulse delay, c is the speed of light, I is the peak intensity, N is the number of cycles in the pulse, and ω_A is the central frequency of the vector potential. ω_A is determined such that the spectral distribution of the E-field matches the given physical central frequency ω_E [59]. The E field is obtained by

$$E(t) = -\frac{1}{c}\frac{\partial}{\partial t}A(t). \quad (5)$$

Once the wave function has been propagated to the end of the pulse we obtain the photoelectron angular distribution by projecting onto numerical continuum states. For an arbitrary radial potential $V(r)$ we propagate the radial Schrödinger equations for a given ℓ from $r = 0$ to $r_{\max}$. Boundary conditions and scattering phase shifts are accounted for via setting $\phi_{k,l}(r = 0) = 0$ and using the asymptotic solution to the Coulomb wave functions

$$\phi_{kl}(r \gg 1) \to \sin\left[kr - \frac{l\pi}{2} + \frac{Z}{k}\ln(2kr) + \delta_{kl}\right]. \quad (6)$$

To normalize the amplitude at $r = r_{\max}$ we set

$$\mathcal{N} = \left[\frac{1}{\sqrt{|\phi_{kl}(r)|^2 + \left|\frac{\phi'_{kl}(r)}{(k+\frac{Z}{kr})}\right|^2}}\right]_{r=r_{\max}} \quad (7)$$

and determine the phase shift δ_{kl} by

$$\delta_{kl} = \left[\arg\left(\frac{i\phi_{kl}(r) + \frac{\phi'_{kl}(r)}{(k+\frac{Z}{kr})}}{(2kr)^{iZ/k}}\right) - kr + \frac{l\pi}{2}\right]_{r=r_{\max}}. \quad (8)$$

The photoelectron angular distribution is then obtained as

$$P_{\mathrm{TDSE}}(k,\theta,\phi) \propto \left|\sum_{l,m} Y^*_{l,m}(\theta,\phi)\int e^{-i\delta_{kl}}(i)^l\phi^*_{kl}(r)\Psi(\boldsymbol{r},t)dr\right|^2. \quad (9)$$

C. Perturbation theory

To reconstruct the initial wave function, i.e., determine amplitudes and phases, we invert the photoelectron angular distributions (here, TDSE results) as a function of time delay by utilizing perturbation theory (PT). In standard perturbation

theory the distribution can be written as

$$P_{\mathrm{PT}}(k,\phi,\tau;\mathbf{a}) \propto \left| a_0 \sum_{\ell,m} \mathcal{A}_0^{\ell,m}(k,\tau) Y_\ell^m\left(\frac{\pi}{2},\phi\right) + \sum_j a_j e^{i\phi_j} \sum_{\ell,m} \mathcal{A}_j^{\ell,m}(k,\tau) Y_\ell^m\left(\frac{\pi}{2},\phi\right) \right|^2, \tag{10}$$

where $\mathbf{a} = \{a_j, \phi_j\}$ is the state vector containing the set of state amplitudes and relative phases, and $\theta = \frac{\pi}{2}$ as only detection of the PADs in the x-y plane is needed for reconstruction of the superpositions considered in the present applications. The signal is normalized in the reconstruction method. Y_ℓ^m are spherical harmonics and $\mathcal{A}_j^{l,m}(k,t)$ is the sum of the first order

$$\mathcal{A}_{\psi_j}^{(1)}(k,t) = \langle \phi_{kl}(t)| \int_{-\infty}^{t} dt_1 G_0(t,t_1) V_{\mathrm{las}}(t_1) |\psi_j(t_1)\rangle \tag{11}$$

and second-order

$$\mathcal{A}_{\psi_j}^{(2)}(k,t) = \langle \phi_{kl}(t)| \int_{-\infty}^{t} dt_1 G_0(t,t_1) V_{\mathrm{las}}(t_1) \times \int_{-\infty}^{t_1} dt_2 G_0(t_1,t_2) V_{\mathrm{las}}(t_2) |\psi_j(t_2)\rangle \tag{12}$$

transition amplitudes from the initial orbital ψ_j where

$$G_0(t,t') = \sum_g \!\!\!\!\!\!\int e^{-iE_g t} |\phi_g(t)\rangle \langle \phi_g(t')| e^{iE_g t'} \tag{13}$$

is the field-free Green's function and

$$V_{\mathrm{las}}(t) = -\mathbf{E}(t)\cdot\mathbf{x} \tag{14}$$

is the electron-field interaction. To evaluate $A_\psi^{(1)}(k,t)$ and $A_\psi^{(2)}(k,t)$ we use the bound states of the TDSE field-free Hamiltonian for the initial states, and expand the Green's function for 200 dipole allowed states per ℓ and m block. The states represent the bound part of the spectrum and a discretized continuum up to an energy of ≈59 eV. The matrix elements and time integrals are performed numerically.

The PT results are then used to obtain a residual

$$R(\mathbf{a}) = \sum_{k,\phi,\tau} \left| \frac{P_{\mathrm{TDSE}}}{\sum_{k,\phi,\tau} |P_{\mathrm{TDSE}}|} - \frac{P_{\mathrm{PT}}(\mathbf{a})}{\sum_{k,\phi,\tau} |P_{\mathrm{PT}}(\mathbf{a})|} \right|^2, \tag{15}$$

where P_{TDSE} and P_{PT} are the TDSE and PT photoelectron distributions for all utilized final momenta, time delays, and detection angles. The state vector $\mathbf{a}$ that minimizes $R(\mathbf{a})$ gives the reconstructed wave function. The normalization maintains the relative yields at each final momentum. To minimize $R(\mathbf{a})$ for the two (three) state system considered below, 1000 (250) evenly spaced samples were used. For the current applications, this minimization technique is sufficient. For superpositions involving more states, the dimensionality of the minimization space increases. It is likely that, for such studies, more advanced minimization methods such as stochastic gradient descent will be needed. We also note that the method is applied to image field-free wave packets, i.e., $\mathbf{a}$ is time independent. For cases in which $\mathbf{a}$ changes with time, an extension of the present method is needed.

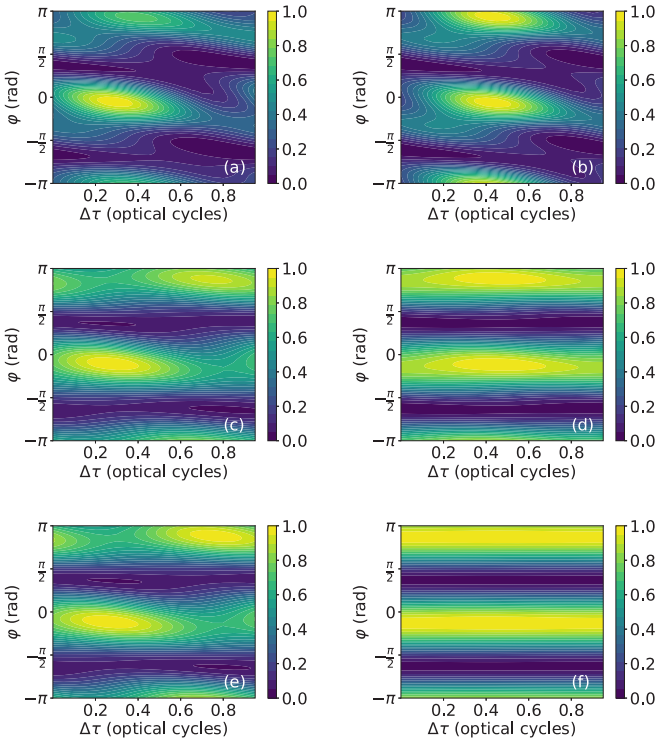

FIG. 2. Results of TDSE calculations for photoelectron angular distributions over one cycle of the probe pulse field for ionization of $1s$-$2p_1$ superposition with ultrashort two-cycle (left column) and ten-cycle (right column) laser pulse with peak intensities of 10^{14} W/cm^2 (top row), 10^{12} W/cm^2 (middle row), and 10^{10} W/cm^2 (bottom row). The time delays $\Delta\tau$ are given with respect to a reference time τ_0 after the end of the first pulse.

III. RESULTS AND DISCUSSION

A. Reconstruction of two-state superposition: Intensity limits and number of samples

To apply the minimization and therefore reconstruct the wave packet, the photoelectron angular distributions (PADs) have to vary as a function of time delay. It is therefore first interesting to see at which laser parameters a significant variation in the PADs can be observed. To this end, in Fig. 2 we show how the PAD varies within one optical cycle of the pump pulse. The delay $\Delta\tau$ in the figure refers to some fixed reference time τ_0 after the end of the first pulse. Comparison of the TDSE results for a two-cycle (≈190 as FWHM, left column) and a ten-cycle (≈950 as FWHM, right column) laser pulse at three peak intensities ranging from 10^{10} W/cm^2 (bottom row) over 10^{12} W/cm^2 (middle row) to 10^{14} (top row) W/cm^2 is shown. In the calculations, the photon energy ω_E has been set to the energy difference between the initially equally populated field-free $1s$ and $2p_1$ states in helium atom $[(|1s\rangle + |2p_1\rangle)/\sqrt{2}]$. We note that, in the present application the energy difference between the two states and the use of transform-limited pulses lead to pulse duration in the attosecond regime. For many other superpositions of atomic states the pump pulse durations will be in the femtosecond regime. The angular distribution is taken at photoelectron energy $E = 2\omega_E - I_p$, where ω_E is the central photon energy and I_p is the ionization energy.

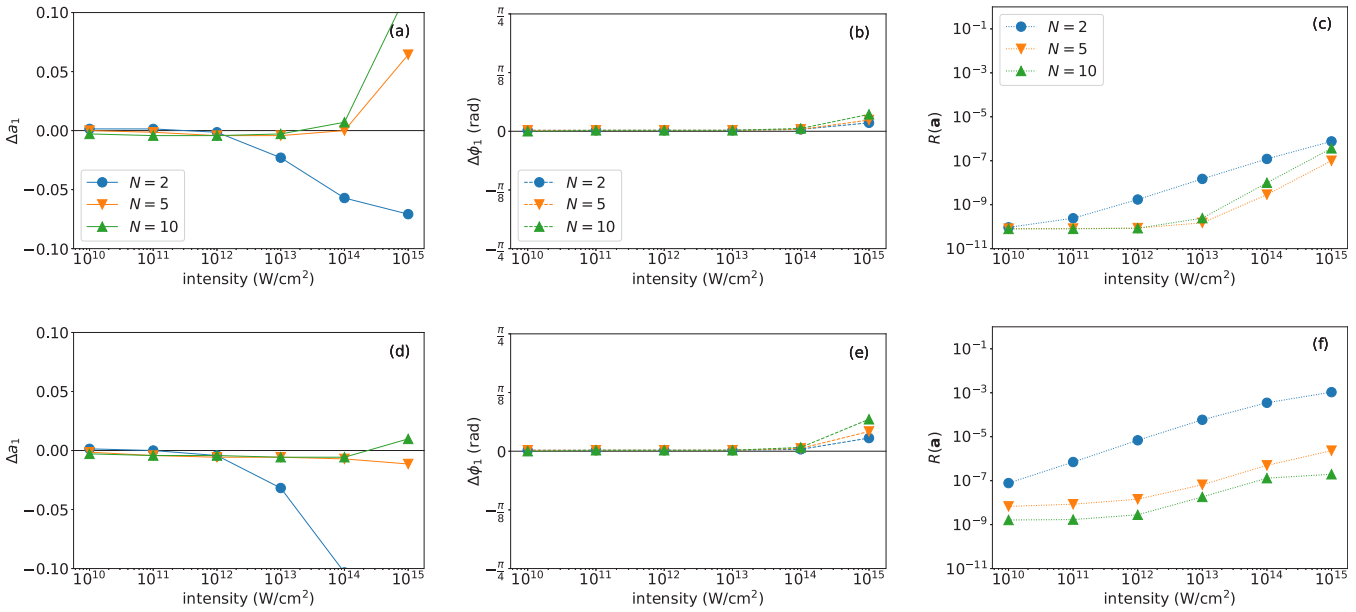

FIG. 3. Errors in (a), (d) amplitude and (b), (e) phase for the two-state reconstruction using PADs generated with laser pulses at two-, five-, and ten-cycle pulse duration. (c), (f) Also shown is the residual $R(\mathbf{a})$. The reconstructions are based on PADs at 20 time samples ($\Delta t = \tau/20$) using PADs in the full x-y plane (upper row) and photoelectron signals in forward-backward direction (lower row).

Although the laser pulse has a FWHM of similar or even longer duration than the charge migration in the present application, the time-delayed PAD shown in Fig. 2 has significant enough variation for the minimization technique to converge. This is due to the coherent nature of the applied laser light. Since the laser is tuned near the resonance, the oscillation of the electric field approximately agrees with that of the superposition to be imaged. This allows for subcycle time dependence to be encoded in the PAD signal.

At the lowest intensity (Fig. 2, bottom row) we observe that the two-cycle signal varies significantly. This is due to the interference between the one-photon ionization channels from the excited state and the ground state. The pathway from the ground state provides a significant contribution to the electron emission due to the broadband spectrum of the ultrashort two-cycle pulse [55,60]. Thus, as the time delay varies, the relative phase of the ground and excited states changes, producing a quantum beating. In contrast, for the longer ten-cycle pulse the spectrum of the pulse is more narrow. Consequently, the contribution from the one-photon pathway from the ground state is much smaller. Hence, the PAD for the ten-cycle pulse at the lowest intensity shows minimal variation as a function of time delay since it is dominated by ionization of the excited state.

As the intensity increases, the relative contribution of the two-photon ionization pathway from the ground state increases because the power dependence of the signals scales with the number of photons absorbed. Since the two-photon channel depends on the absorption of photons at the central energy the significance of the contribution does not depend on the pulse duration. As a result, we observe that, at the largest intensity considered in Fig. 2 (top row), both the two- and the ten-cycle PADs vary strongly as functions of time delay. This is due to the interference between the one-photon ionization from the excited state and the two-photon ionization from the ground state.

To demonstrate the reconstruction method the errors in reconstructing the amplitude and phase of the superposition state $(|1s\rangle + |2p_+\rangle)/\sqrt{2}$ in helium atom as a function of peak intensity are shown in Figs. 3(a), 3(d) and 3(b), 3(e), respectively. The error is obtained via $\Delta a = a' - a$, where a is the amplitude or phase of the original wave function and a' is the corresponding amplitude or phase of the reconstructed wave function. The reconstruction is based on PADs taken at 20 time delays over one period of quantum beating $\tau = 2\pi/|E_{2p_1} - E_{1s}|$. Also shown are the final results of the minimization for $R(\mathbf{a})$ [Figs. 3(c) and 3(f)].

Reconstructions of two cases are compared in which either the full PAD in the x-y plane via signals at 6285 equally spaced angles (upper row) or only the signals in the forward-backward direction along the polarization axis of the probe pulse (lower row) are used. The results in the upper row show that the reconstruction method reproduces the initial state up to peak laser intensities of about 10^{13} W/cm^2 if the full x-y plane and 20 time samples are used. The increase of the errors at intensities larger than 10^{13} W/cm^2 indicates that higher-order processes begin to contribute leading to the breakdown of the present second-order reconstruction method. For a two-state superposition, just two amplitudes and the relative phase have to be determined. Using the full PAD with several thousand signals is oversampling for the reconstruction method. This is confirmed by the results for the reconstruction [Figs. 3(d) and 3(f)] using the PAD signals in forward-backward direction only.

Next, we studied if one can limit the number of PAD samples over time. Toward this end, we present in Fig. 4 the errors in amplitude and phase based on a reconstruction using just two PADs over one period of quantum beating

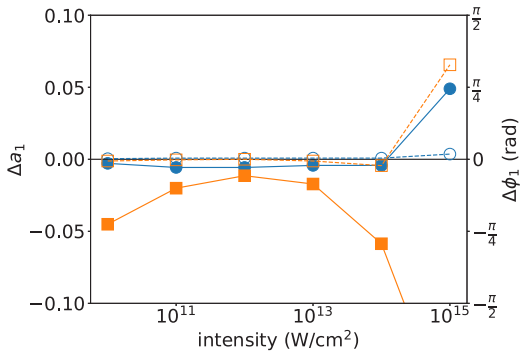

FIG. 4. Same as Fig. 3 but based on PADs at just two time delays. Errors in amplitude (filled symbols with solid lines) and phase (open symbols with dashed lines) are shown for using PADs in the full x-y plane (blue squares) and in the forward-backward direction (orange circles).

$\tau = 2\pi/|E_{2p_1} - E_{1s}|$. If the full PAD in the x-y plane is used (blue squares), the reconstruction method remains successful over the same intensity regime as before. However, when the available signals are limited to the forward-backward direction (orange circles), the data are insufficient for a one-to-one mapping between the initial state and the obtained photoelectron signal. Consequently, the reconstruction fails at nearly all peak laser intensities, since for just two time samples the normalization leads to a greater chance that multiple values for amplitudes and the relative phase produce a given signal.

Thus, for the basic case of equal population in a two-state superposition and probing with a pulse having a central frequency equal to the field-free energy difference of the state, our results show that the reconstruction method is successful for intensities in the perturbative regime up to 10^{13} W/cm^2. If the PADs can be measured over a broad range of angles probing at two times over one cycle of the probe pulse field is sufficient. In contrast, if only the forward-backward asymmetry signals are measured more time samples are needed.

B. Impact of different pathways

The reconstruction depends on the effective interference of at least two amplitudes to have a quantum beating. In the full reconstruction we consider the contributions from four pathways (one- and two-photon transitions from ground and excited states). It is interesting to ask which pathways contribute effectively besides the one-photon transition from the excited state. To study this question, we have deliberately neglected individual amplitudes in the reconstruction. In Fig. 5 we compare the results of these calculations with those of the full reconstruction (blue bars) based on the full x-y plane and 20 time samples. We show the results for the amplitude error only and note that those for the phase error lead to the same conclusions.

We performed two set of test calculations: First, we utilized all amplitudes except the two-photon signal from the excited state (orange bars). Next, we removed the one-photon signal from the ground state and the two-photon signal from the excited state from the reconstruction (green bars). Both transition amplitudes are expected to have an impact at

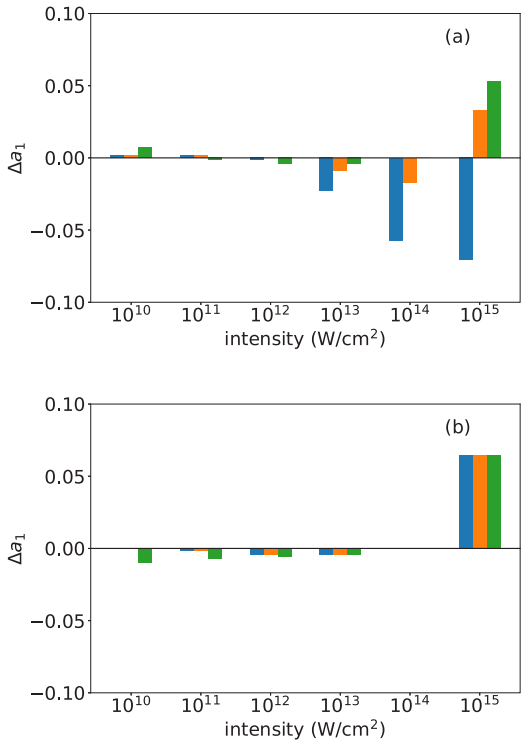

FIG. 5. Comparison of amplitude error for a (a) two- and (b) five-cycle probe pulse from calculations using full second-order PT (blue), neglecting only the two-photon transition from the excited state (orange) and neglecting both the one-photon transition from the ground state and the two-photon amplitude from the excited state (green) in the reconstruction.

ultrashort durations due to the broad bandwidth of the pulses. Indeed, we do see noticeable changes for the two-cycle data [Fig. 5(a)] while there appears to be insignificant impact for the five-cycle pulse [Fig. 5(b)] at all intensities.

For a two-cycle probe pulse, at intensities less than 10^{13} W/cm^2, the reconstruction without the two-photon amplitude from the excited state matches the full data [Fig. 3(a)]. At higher intensities, the results deviate, which agrees with the expectation. Removing also the one-photon transition from the ground state from the reconstruction causes the results to deviate from the full results at 10^{10} W/cm^2 and above 10^{13} W/cm^2. At the lowest intensity it is the one-photon signal from the ground state that provides a dominant contribution to the PAD, leading to the deviation at 10^{10} W/cm^2. At intensities above 10^{13} W/cm^2, the additional exclusion of the one-photon signal leads to a better reconstruction than for the full data and when the two-photon pathway from the excited state is neglected. This can indicate that inadvertently the two ultrashort amplitudes have an opposite effect on the reconstruction or that an even higher-order amplitude is more dominant than the lower-order processes.

C. Variation of central frequency and population

So far, we have considered a special case with equal population in the two states and the central frequency tuned to the energy difference between the two field-free states. We will now study deviations from this special case. First, we consider

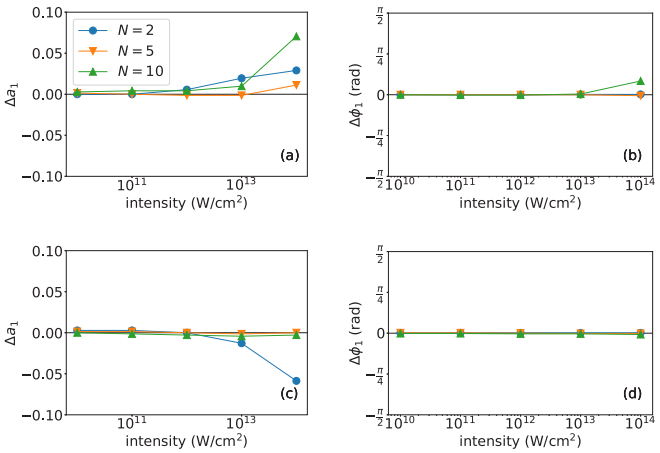

FIG. 6. (a), (c) Amplitude and (b), (d) phase errors for ionization at a detuned photon frequency of $\omega = 0.8\omega_0$ (upper row) and $\omega = 1.2\omega_0$ (lower row). The reconstructions are based on full PADs in x-y plane at 20 time delays.

a laser pulse detuned from the energy difference between the two equally populated states. We calculated the photoelectron distribution at $E = \omega_E - |E_e|$, where E_e is the energy of the excited $2p_1$ state. Given a sufficiently broad spectral range, i.e., sufficiently short pulse, the one-photon ground-state signal (peaking at about $E = \omega_E - |E_g|$) at low intensities will interfere with the excited-state signal creating the same quantum beating as before allowing for the reconstruction process to work. In Fig. 6 we show the reconstruction results for a laser with central frequency of $\omega_E = 0.8\omega_0$ (upper row) and $\omega_E = 1.2\omega_0$ (lower row). The results lead to the same conclusion as for the resonant case, namely, that the reconstruction method can be applied in the perturbative intensity regime up to 10^{13} W/cm^2.

To show that the reconstruction works for a two-state superposition with arbitrary unknown amplitudes and phases, we have performed a "blindfold experiment" where the population of the states were chosen randomly. The random values were held unknown and were only accessed to obtain the final error at the end of the reconstruction procedure. We have used this approach in several calculations and for probe pulses of different duration, with results leading to the same conclusion. As an example, one set of results for this blindfold experiment is presented in Fig. 7, showing that the reconstruction is successful with the same low errors as in the other cases studied.

D. Detector accuracy and variation of laser parameters

For the reconstructions so far we have used results from TDSE calculations up to machine precision. Since detectors in experiment do not operate with the same precision we have studied how less accurate data may impact the success of the reconstruction. To this end, we have deliberately added random noise at a certain percentage level of the maximum signal in the PADs to the TDSE data. In Fig. 8 we compare the results for the reconstruction with added noise at the 1% and 10% level with those at machine precision using the signals from the full x-y plane and 20 time samples. It is seen that an accuracy of detection at the 1% level is sufficient

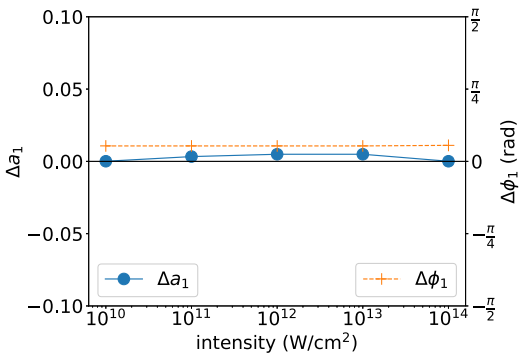

FIG. 7. Amplitude and phase error for the reconstruction of an arbitrary unknown two-state superposition. Reconstruction is based on full PADs in the x-y plane at 20 time delays with a five-cycle probe pulse.

to reconstruct the wave function with similar error as in the full calculation with TDSE data at machine precision. Similar results and conclusions have been obtained for the other cases presented in Figs. 3 and 4. We expect that this limit can be achieved in a measurement.

We have further considered variations in the laser parameters relevant for an application of the reconstruction method in an experiment. Typically, the peak intensity of the applied laser pulse may vary from shot to shot as well as over the interaction volume. Another parameter that is usually difficult to control is the carrier-to-envelope phase (CEP) of a laser pulse, specifically for ultrashort pulses. To study the impact on the reconstruction, CEP, peak intensity, and both CEP and

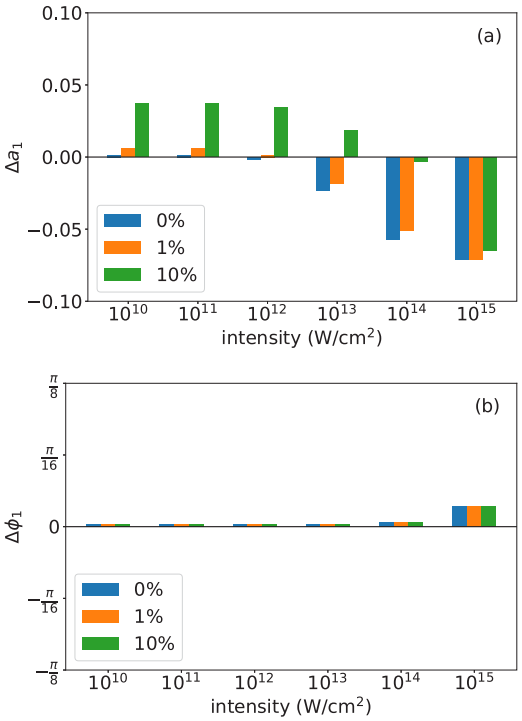

FIG. 8. Comparison of (a) amplitude and (b) phase error for reconstruction using PADs at machine precision (blue) and with accuracy limited to 1% and 10%.

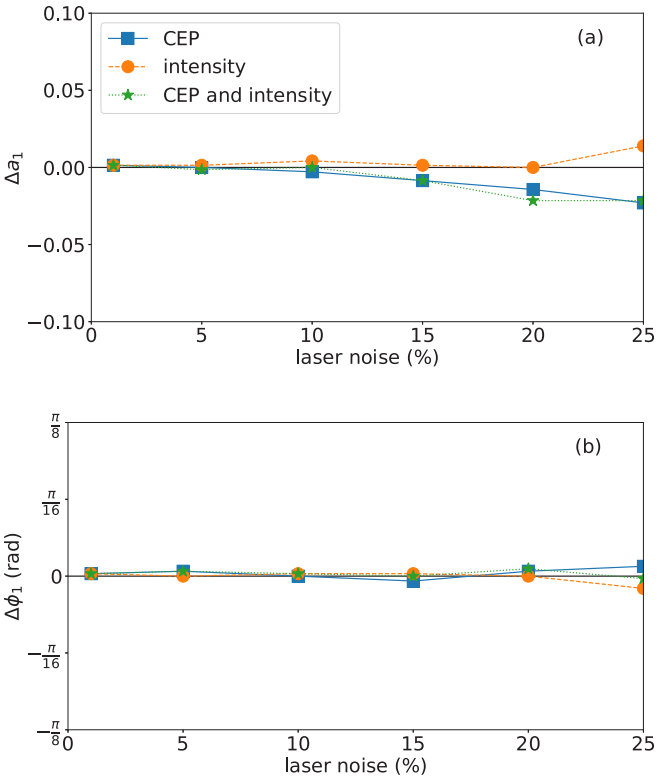

FIG. 9. (a) Amplitude and (b) phase error for variation of CEP only (blue squares with solid lines), intensity only (orange circles with dashed lines) and both CEP and intensity (green stars with dotted lines) at peak intensity of 10^{11} W/cm^2 and pulse duration of two cycles. Reconstruction is based on full PADs in x-y plane at 20 time delays.

peak intensity have been varied randomly within a certain percentage in the TDSE results. The results in Fig. 9 show that the reconstruction method still works well up to 10% variation in both parameters before significant errors occur. Perhaps most surprising is the rather large acceptable tolerance in the CEP even for the shortest pulses, since CEP variations often lead to large changes in experimental observables. We assume that the shot to shot variation is "averaging out" over the various time delays leading to a quality in the reconstruction similar to fitting a linear regression to noisy data.

E. Extension to superpositions of more than two states

Finally, we consider the extension of the reconstruction method to a superposition of more than two states. The ionization scheme shown in Figs. 1(c) and 1(d) can be applied to each excited state in the superposition separately, taking the waves generated via one- and two-photon transitions from the ground state as reference. For the reconstruction measurement of PADs at separate energies for each excited state in the superposition is required. Based on PT results, residuals $R(\mathbf{a})$ [Eq. (15)] have been obtained, taking into account both final momenta to reconstruct the wave function.

To test the extension of the method we have considered the helium atom in the $(|1s\rangle + |2p_1\rangle + |3p_1\rangle)/\sqrt{3}$ superposition. A probe laser pulse at central photon energy tuned halfway between the $|2p_1\rangle$ and $|3p_1\rangle$ states and measurement of PADs

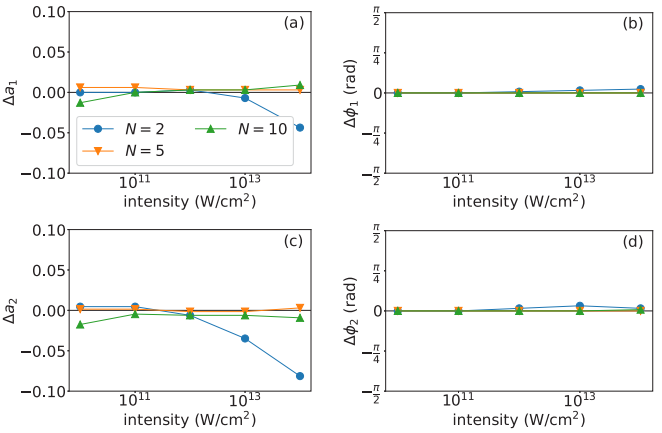

FIG. 10. (a), (c) Amplitude and (b), (d) phase errors for the reconstruction of the superposition $(|1s\rangle + |2p_1\rangle + |3p_1\rangle)/\sqrt{3}$ in the helium atom (upper row: errors for $2p$ state, lower row: errors for $3p$ state).

at both $E = \omega - |E_{2p}|$ and $E = \omega - |E_{3p}|$ have been applied. The results of the reconstruction, based on PADs in the full x-y plane taken at 20 time delays, are shown as function of peak intensity for different pulse durations in Fig. 10. The results show that a similar degree of accuracy in the reconstruction as for the two-state superposition is achieved within the same intensity limits. The example indicates that the present method may be extended to even more complex wave packets and electron dynamics.

Extension of the reconstruction method to more complex superpositions will require attention to the interference with the ground-state signal and the increased dimensionality of the minimization space. Since the minimization process appears to be convex, a standard minimization algorithm, like conjugate gradient, may be sufficient for an efficient reconstruction. For each additional state in the interference scheme, the signal at the photoelectron energy chosen must include interference with at least one other state. This can be achieved if all transitions from the excited states interfere with that from the ground state by using a short pulse. If only longer pulses are available, coupling over many pairs of states reduces the required bandwidth for a reconstruction. Finally, due to the selection rules some initial states do not generate a signal in the xy plane. In this case it may be required to utilize a full 4π PAD for reconstruction of the corresponding superposition.

IV. SUMMARY AND OUTLOOK

We have studied the use of perturbation theory to reconstruct an atomic wave function representing ultrafast field-free charge migration. In the reconstruction scheme the photoelectron angular distributions obtained by ionizing an atom, prepared in a superposition of two or three states, are used. The electron dynamics are encoded in the PAD signal via interference of the ground and excited-state ionization signals. Time delayed measurements allow for the extraction of all amplitudes and phases of the initial wave function that fully characterizes the charge migration. Results of applications based on TDSE calculations show that the reconstruction is highly accurate for probe pulse intensities below 10^{13} W/cm^2

while allowing for CEP (intensity) variations of 10% (20%) from shot to shot. Additionally, a detection accuracy for the PADs of about 1% for a reconstruction with small error is required.

These results may provide some basic guidelines for future experimental progress in imaging electron motion on its fundamental timescale via the detection of photoelectron angular distributions. However, the results also show that experimental challenges remain. Controlling the creation of ultrashort laser pulses, especially those with attosecond pulse duration, is a nontrivial task. For the current method to be applied, average values for intensity, CEP and pulse duration of the electric field of the probe pulse must be obtained and shot-to-shot variations must be limited up to a certain degree. Given the rate of advancement in attosecond laser pulse technology over the last decade, this level of pulse control may be however achieved in the coming years.

Additionally, precise knowledge of one- and two-photon transition dipoles is required to perform perturbation theory calculations for the target atom with high accuracy. Over the last decades several standard theoretical methods, such as multielectron theories, density-functional theory or calculations using accurate single active electron potentials, have been developed to perform such calculations. As theoretical methods for bound and continuum wave functions further advance, the current and other reconstruction methods will become increasingly accurate.

ACKNOWLEDGMENTS

We thank Tennesse Joyce for useful discussions concerning the projection on continuum states. This work was primarily supported (J.V., A.B.) by a grant from the U.S. Department of Energy, Division of Chemical Sciences, Atomic, Molecular and Optical Sciences Program (Award No. DE-SC0001771). A.J.-B. acknowledges support by a grant from the U.S. National Science Foundation (Grant No. PHY-1734006).

[1] E. A. Seddon, J. A. Clarke, D. J. Dunning, C. Masciovecchio, C. J. Milne, F. Parmigiani, D. Rugg, J. C. H. Spence, N. R. Thompson, K. Ueda *et al.*, Rep. Prog. Phys. **80**, 115901 (2017).
[2] T. Popmintchev, M.-C. Chen, P. Arpin, M. M. Murnane, and H. C. Kapteyn, Nat. Photonics **4**, 822 (2010).
[3] M. Chini, K. Zhao, and Z. Chang, Nat. Photonics **8**, 178 (2014).
[4] K. Zhao, Q. Zhang, M. Chini, Y. Wu, X. Wang, and Z. Chang, Opt. Lett. **37**, 3891 (2012).
[5] M.-C. Chen, C. Mancuso, C. Hernández-García, F. Dollar, B. Galloway, D. Popmintchev, P.-C. Huang, B. Walker, L. Plaja, A. A. Jaroń-Becker *et al.*, Proc. Natl. Acad. Sci. USA **111**, E2361 (2014).
[6] M. J. J. Vrakking, Phys. Chem. Chem. Phys. **16**, 2775 (2014).
[7] R. Pazourek, S. Nagele, and J. Burgdörfer, Rev. Mod. Phys. **87**, 765 (2015).
[8] F. Calegari, G. Sansone, S. Stagira, C. Vozzi, and M. Nisoli, J. Phys. B: At., Mol. Opt. Phys. **49**, 062001 (2016).
[9] K. Ramasesha, S. R. Leone, and D. M. Neumark, Annu. Rev. Phys. Chem. **67**, 41 (2016).
[10] L. Young, K. Ueda, M. Gühr, P. H. Bucksbaum, M. Simon, S. Mukamel, N. Rohringer, K. C. Prince, C. Masciovecchio, M. Meyer *et al.*, J. Phys. B: At., Mol. Opt. Phys. **51**, 032003 (2018).
[11] P. Peng, C. Marceau, and D. M. Villeneuve, Nat. Rev. Phys. **1**, 144 (2019).
[12] A. L. Cavalieri, N. Müller, T. Uphues, V. S. Yakovlev, A. Baltuška, B. Horvath, B. Schmidt, L. Blümel, R. Holzwarth, S. Hendel *et al.*, Nature (London) **449**, 1029 (2007).
[13] M. Schultze, M. Fieß, N. Karpowicz, J. Gagnon, M. Korbman, M. Hofstetter, S. Neppl, A. L. Cavalieri, Y. Komninos, T. Mercouris *et al.*, Science **328**, 1658 (2010).
[14] K. Klünder, J. M. Dahlström, M. Gisselbrecht, T. Fordell, M. Swoboda, D. Guénot, P. Johnsson, J. Caillat, J. Mauritsson, A. Maquet *et al.*, Phys. Rev. Lett. **106**, 143002 (2011).
[15] Z. Tao, C. Chen, T. Szilvási, M. Keller, M. Mavrikakis, H. Kapteyn, and M. Murnane, Science **353**, 62 (2016).
[16] M. Isinger, R. J. Squibb, D. Busto, S. Zhong, A. Harth, D. Kroon, S. Nandi, C. L. Arnold, M. Miranda, J. M. Dahlström *et al.*, Science **358**, 893 (2017).
[17] J. Su, H. Ni, A. Jaroń Becker, and A. Becker, Phys. Rev. Lett. **113**, 263002 (2014).
[18] M. Sabbar, S. Heuser, R. Boge, M. Lucchini, T. Carette, E. Lindroth, L. Gallmann, C. Cirelli, and U. Keller, Phys. Rev. Lett. **115**, 133001 (2015).
[19] X. Gong, C. Lin, F. He, Q. Song, K. Lin, Q. Ji, W. Zhang, J. Ma, P. Lu, Y. Liu *et al.*, Phys. Rev. Lett. **118**, 143203 (2017).
[20] A. Jiménez-Galán, L. Argenti, and F. Martín, Phys. Rev. Lett. **113**, 263001 (2014).
[21] V. K. Dolmatov, A. S. Kheifets, P. C. Deshmukh, and S. T. Manson, Phys. Rev. A **91**, 053415 (2015).
[22] L. Barreau, C. L. M. Petersson, M. Klinker, A. Camper, C. Marante, T. Gorman, D. Kiesewetter, L. Argenti, P. Agostini, J. González-Vázquez *et al.*, Phys. Rev. Lett. **122**, 253203 (2019).
[23] A. Kaldun, A. Blättermann, V. Stooß, S. Donsa, H. Wei, R. Pazourek, S. Nagele, C. Ott, C. D. Lin, J. Burgdörfer *et al.*, Science **354**, 738 (2016).
[24] M. Kotur, D. Guénot, Á. Jiménez-Galán, D. Kroon, E. W. Larsen, M. Louisy, S. Bengtsson, M. Miranda, J. Mauritsson, C. L. Arnold *et al.*, Nat. Commun. **7**, 10566 (2016).
[25] V. Gruson, L. Barreau, Á. Jimnez-Galan, F. Risoud, J. Caillat, A. Maquet, B. Carré, F. Lepetit, J.-F. Hergott, T. Ruchon *et al.*, Science **354**, 734 (2016).
[26] C. Cirelli, C. Marante, S. Heuser, C. L. M. Petersson, Á. Jiménez-Galán, L. Argenti, S. Zhong, D. Busto, M. Isinger, S. Nandi *et al.*, Nat. Commun. **9**, 955 (2018).
[27] A. N. Pfeiffer, C. Cirelli, M. Smolarski, R. Dörner, and U. Keller, Nat. Phys. **7**, 428 (2011).
[28] R. Pazourek, J. Feist, S. Nagele, and J. Burgdörfer, Phys. Rev. Lett. **108**, 163001 (2012).
[29] E. P. Månsson, D. Guénot, C. L. Arnold, D. Kroon, S. Kasper, J. M. Dahlström, E. Lindroth, A. S. Kheifets, A. L'Huillier, S. L. Sorensen *et al.*, Nat. Phys. **10**, 207 (2014).
[30] E. Goulielmakis, Z.-H. Loh, A. Wirth, R. Santra, N. Rohringer, V. S. Yakovlev, S. Zherebtsov, T. Pfeifer, A. M. Azzeer, M. F. Kling *et al.*, Nature (London) **466**, 739 (2010).

[31] J. Mauritsson, T. Remetter, M. Swoboda, K. Klünder, A. L'Huillier, K. J. Schafer, O. Ghafur, F. Kelkensberg, W. Siu, P. Johnsson *et al.*, Phys. Rev. Lett. **105**, 053001 (2010).
[32] M. Holler, F. Schapper, L. Gallmann, and U. Keller, Phys. Rev. Lett. **106**, 123601 (2011).
[33] P. Hockett, C. Z. Bisgaard, O. J. Clarkin, and A. Stolow, Nat. Phys. **7**, 612 (2011).
[34] K. T. Kim, D. H. Ko, J. Park, N. N. Choi, C. M. Kim, K. L. Ishikawa, J. Lee, and C. H. Nam, Phys. Rev. Lett. **108**, 093001 (2012).
[35] X. Xie, S. Roither, D. Kartashov, E. Persson, D. G. Arbó, L. Zhang, S. Gräfe, M. S. Schöffler, J. Burgdörfer, A. Baltuška *et al.*, Phys. Rev. Lett. **108**, 193004 (2012).
[36] K. Klünder, P. Johnsson, M. Swoboda, A. L'Huillier, G. Sansone, M. Nisoli, M. J. J. Vrakking, K. J. Schafer, and J. Mauritsson, Phys. Rev. A **88**, 033404 (2013).
[37] A. R. Beck, B. Bernhardt, E. R. Warrick, M. Wu, S. Chen, M. B. Gaarde, K. J. Schafer, D. M. Neumark, and S. R. Leone, New J. Phys. **16**, 113016 (2014).
[38] M. T. Hassan, T. T. Luu, A. Moulet, O. Raskazovskaya, P. Zhokhov, M. Garg, N. Karpowicz, A. M. Zheltikov, V. Pervak, F. Krausz *et al.*, Nature (London) **530**, 66 (2016).
[39] S. G. Walt, N. B. Ram, M. Atala, N. I. Shvetsov-Shilovski, A. von Conta, D. Baykusheva, M. Lein, and H. J. Wörner, Nat. Commun. **8**, 15651 (2017).
[40] K. E. Priebe, C. Rathje, S. V. Yalunin, T. Hohage, A. Feist, S. Schäfer, and C. Ropers, Nat. Photonics **11**, 793 (2017).
[41] M. He, Y. Li, Y. Zhou, M. Li, W. Cao, and P. Lu, Phys. Rev. Lett. **120**, 133204 (2018).
[42] S. X. Hu and L. A. Collins, Phys. Rev. Lett. **96**, 073004 (2006).
[43] J. Feist, S. Nagele, C. Ticknor, B. I. Schneider, L. A. Collins, and J. Burgdörfer, Phys. Rev. Lett. **107**, 093005 (2011).
[44] C. Ott, A. Kaldun, L. Argenti, P. Raith, K. Meyer, M. Laux, Y. Zhang, A. Blättermann, S. Hagstotz, T. Ding *et al.*, Nature (London) **516**, 374 (2014).
[45] H. Eichmann, A. Egbert, S. Nolte, C. Momma, B. Wellegehausen, W. Becker, S. Long, and J. K. McIver, Phys. Rev. A **51**, 3414(R) (1995).
[46] A. Fleischer, O. Kfir, T. Diskin, P. Sidorenko, and O. Cohen, Nat. Photonics **8**, 543 (2014).
[47] T. Fan, P. Grychtol, R. Knut, C. Hernández-García, D. D. Hickstein, D. Zusin, C. Gentry, F. J. Dollar, C. A. Mancuso, C. W. Hogle *et al.*, Proc. Natl. Acad. Sci. USA **112**, 14206 (2015).
[48] D. D. Hickstein, F. J. Dollar, P. Grychtol, J. L. Ellis, R. Knut, C. Hernández-García, D. Zusin, C. Gentry, J. M. Shaw, T. Fan *et al.*, Nat. Photonics **9**, 743 (2015).
[49] P.-C. Huang, C. Hernández-García, J.-T. Huang, P.-Y. Huang, C.-H. Lu, L. Rego, D. D. Hickstein, J. L. Ellis, A. Jaron-Becker, A. Becker *et al.*, Nat. Photonics **12**, 349 (2018).
[50] C. Spezzani, E. Allaria, M. Coreno, B. Diviacco, E. Ferrari, G. Geloni, E. Karantzoulis, B. Mahieu, M. Vento, and G. De Ninno, Phys. Rev. Lett. **107**, 084801 (2011).
[51] T. Mazza, M. Ilchen, A. J. Rafipoor, C. Callegari, P. Finetti, O. Plekan, K. C. Prince, R. Richter, M. B. Danailov, A. Demidovich *et al.*, Nat. Commun. **5**, 3648 (2014).
[52] P. M. Paul, E. S. Toma, P. Breger, G. Mullot, F. Augé, P. Balcou, H. G. Muller, and P. Agostini, Science **292**, 1689 (2001).
[53] H. G. Muller, Appl. Phys. B: Lasers Opt. **74**, s17 (2002).
[54] W.-C. Jiang, X.-M. Tong, R. Pazourek, S. Nagele, and J. Burgdörfer, Phys. Rev. A **101**, 053435 (2020).
[55] J. Venzke, A. Jaroń-Becker, and A. Becker, J. Phys. B: At., Mol. Opt. Phys. **53**, 085602 (2020).
[56] R. Reiff, T. Joyce, A. Jaron-Becker, and A. Becker, J. Phys. Commun. **4**, 065011 (2020).
[57] A. Scrinzi, Phys. Rev. A **81**, 053845 (2010).
[58] S. Chelkowski and A. D. Bandrauk, Phys. Rev. A **65**, 061802(R) (2002).
[59] J. Venzke, T. Joyce, Z. Xue, A. Becker, and A. Jaron-Becker, Phys. Rev. A **98**, 063409 (2018).
[60] J. Venzke, A. Becker, and A. Jaron-Becker, Sci. Rep. **10**, 16164 (2020).